

Light-matter correlations in Quantum Floquet engineering

Beatriz Pérez-González,^{1,*} Gloria Platero,^{1,†} and Álvaro Gómez-León^{2,‡}

¹*Instituto de Ciencia de Materiales de Madrid (ICMM), CSIC,
Calle Sor Juana Inés de la Cruz 3, 28049 Madrid, Spain*

²*Instituto de Física Fundamental (IFF), CSIC, Calle Serrano 113b, 28006 Madrid, Spain.*

(Dated: February 27, 2023)

Quantum Floquet engineering requires a proper gauge-invariant description of light-matter interaction to correctly capture the physics of the system beyond the strong-coupling regime. This means that such models typically involve a highly non-linear dependence on the photonic operators which makes their analysis and simulation complex. In this work, we provide a non-perturbative truncation scheme for the light-matter Hamiltonian, which is valid for arbitrary coupling strength. Within this framework, we investigate the crucial role of light-matter correlations, which are absent in a classical Floquet description. We find that, even in the high-frequency regime, they can spontaneously break key symmetries for topological protection, and be detected in the photonic spectral function. We exemplify our findings with the SSH chain, and show that a topological phase transition can be induced by coupling to a cavity and that the critical point can be predicted from the spectral function.

Since the earliest studies to understand the nature of light, harnessing light-matter interactions has been a persistent goal in condensed matter physics and, more recently, in quantum technologies.

A well-known example is the use of classical driving fields as external knobs to alter and control the properties of materials, in what is now widely known as *Floquet engineering* [1, 2]. In this case, outstanding experiments have demonstrated that classical light can induce non-trivial topology [3], or create non-equilibrium phases without a static counterpart [4]. Nevertheless, this external control comes with a cost, as the energy of the classical field produces unavoidable heating that spoils the emergent physics of Floquet engineering [5–7], unless additional strategies are adopted [8–11].

An avenue currently being explored [12–14], known as *Quantum Floquet engineering* [15, 16], involves the use of quantum fields rather than classical ones.

Although in certain limits it shares some similarities with classical Floquet engineering [15], the back-action between the quantum system and the photon field or the existence of light-matter correlations can lead to physics beyond that of classical Floquet engineering. In addition, with quantum light the problem of heating can be mitigated, as the whole system is approximately isolated from its environment.

As in its classical counterpart, creating new phases in Quantum Floquet engineering sometimes requires reaching large coupling strengths [17]. This poses new technological challenges, and among them, the achievement of light-matter interaction beyond the strong coupling regime especially stands out. Although it has been shown that it is within experimental reach [18, 19]. Theoretically, this regime also entails some difficulties. It was recently revealed that describing regimes where the interac-

tion strength is of the order of the transition frequencies of the system requires including the photonic field operators to arbitrary order in the Hamiltonian [20–24]. Unfortunately, such Hamiltonians are extremely non-linear and complex to simulate. This makes it important to develop effective models which can describe the system over a wide range of coupling regimes, being also simple enough to capture the main mechanisms governing the physics.

In this work, we present a framework to obtain simple effective Hamiltonians by means of a disentangling technique [25]. It allows us to find a non-perturbative, polynomial expansion of the full, gauge-invariant Hamiltonian, which can be truncated to low order and provides accurate results for arbitrary coupling strength.

Within this framework, we study the paradigmatic case of a Su-Schrieffer-Heeger (SSH) chain [26, 27] coupled to a single mode cavity, and show that their interaction can produce topological phase transitions. Interestingly, each photonic band exhibits its own topological phase transitions, which allows the control of the topological properties of the fermionic system through the number of cavity photons. Furthermore, we find that light-matter correlations are crucial as they can spontaneously break chiral symmetry, severely affecting the topology even when the cavity frequency is far detuned from the electronic system. Recent experiments have found the breaking of topological protection due to the interaction with cavity fields [28]. With these results in mind, we address the important differences between classical and quantum Floquet engineering in the high frequency regime.

Finally, we discuss how the spectroscopy of the photons can be used to detect all our findings and the possibility to use the cavity to externally control the state transfer between topological edge states.

Results

Model. Consider a tight binding description of spinless fermions in a lattice, coupled to a single-mode cavity. The quantized electric field in the cavity can be expressed in terms of the vector potential $\vec{A} = A_0 (d + d^\dagger) \hat{u}(r)$, where \hat{u} is the unitary polarization vector, $A_0 = 1/\sqrt{2\varepsilon_0\Omega\nu}$ ($\hbar = 1$), ε_0 is the vacuum permittivity, Ω the cavity frequency, and ν the mode volume [29]. In the Coulomb gauge and under a dipole approximation, the coupling between the two systems can be introduced via the Peierls substitution (see Methods), which yields the total Hamiltonian [30]:

$$H = \Omega d^\dagger d + \sum_{l,j=1}^N J_{l,j} e^{i\phi_{l,j}} c_l^\dagger c_j, \quad (1)$$

with N the number of sites in the array and $J_{l,j}$ the hopping. The creation/annihilation operators c_j^\dagger/c_j are fermionic, while d/d^\dagger are bosonic. The fermionic hopping amplitudes are dressed by the Peierls phase, $\phi_{l,j} = \eta_{l,j} (d^\dagger + d)$, with $\eta_{l,j} = eA_0 r_{l,j}$ acting as the effective coupling strength (e is the particle charge and $r_{l,j}$ is the distance between the l^{th} and j^{th} site). Importantly, notice that since $r_{l,j} = -r_{j,l}$, the coupling $\eta_{j,l}$ depends on both the distance between sites and the direction of the hopping.

Eq. (1) represents a gauge invariant description of the system for arbitrary coupling strength, but it is also highly non-linear in the photonic operators, which makes its use difficult for practical calculations. A standard maneuver to make Eq. (1) more manageable is based on the early studies of polaron physics [25, 31]. There, the use of the Baker-Hausdorff-Campbell formula, in combination with the Hubbard operators, $Y^{n,n'} = |n\rangle\langle n'|$, with $n, n' \in \mathbb{Z} \geq 0$ and $|n\rangle$ the number of particle states, allows us to write the Peierls phase term as:

$$e^{i\eta_{l,j}(d^\dagger + d)} = \sum_{n=0}^{\infty} g_{n,n}^{l,j} Y^{n,n} + \sum_{n \neq m=0}^{\infty} g_{m,n}^{l,j} Y^{m,n}, \quad (2)$$

where $g_{s,s}^{l,j} = e^{-\eta_{l,j}^2/2} L_s(\eta_{l,j}^2)$, $L_s(\eta_{l,j}^2)$ are the Laguerre polynomials, and where the off-diagonal terms are given by the Hypergeometric functions ${}_1F_1(s, l, \eta_{l,j}^2)$ (see Methods) [32]:

$$g_{s,l}^{l,j} = e^{-\eta_{l,j}^2/2} \frac{(i\eta_{l,j})^{l-s}}{(l-s)!} \sqrt{\frac{l!}{s!}} {}_1F_1(s, l, \eta_{l,j}^2). \quad (3)$$

After all these manipulations we can rewrite Eq. (1) as:

$$H = \sum_{n=0}^{\infty} (n\Omega + \sum_{\langle j,l \rangle=1}^N g_{n,n}^{l,j} J_{j,l} c_j^\dagger c_l) Y^{n,n} + \sum_{n \neq m=0}^{\infty} \sum_{\langle j,l \rangle=1}^N g_{m,n}^{l,j} J_{j,l} c_j^\dagger c_l Y^{m,n}, \quad (4)$$

where the first line can be interpreted as a state-dependent frequency shift and the second as photon-assisted hopping. Eq. (4) has the advantage of being a non-perturbative polynomial expansion in photon operators, and we will show that even after truncation, it is still accurate in the case of ultrastrong coupling.

Eq. (4) is valid for arbitrary 1D lattices coupled to photons. However, here we are interested in systems with non-trivial topology, either in the unperturbed fermionic system or in the emergent many-body phase. For this reason, we focus on a bipartite lattice or SSH chain [26, 27]. This system is characterized by the ratio between the intra- and the inter-dimer hopping amplitudes, $J_{2j-1,2j} = J_{2j,2j-1} \equiv J'$ and $J_{2j,2j+1} = J_{2j+1,2j} \equiv J$, respectively (see Methods). Notice that the hopping dimerization can be accompanied by a different intra/inter-dimer distance, r' and r (the unit cell length is set to $r + r' = 1$), with well-known physical consequences in classical Floquet engineering [33]. This leads to a dimerized interaction strength that depends on either r or r' : $\eta^{(r)} = eA_0 r^{(r)}$. In the following, we will present the results of our calculations as a function of η (η' can be directly obtained from $\eta' = \eta r'/r$).

Having particularized Eq. (4) to the SSH model, we now simplify its form by truncating the number of photons that can be exchanged during transitions. We assume that in our case of interest, only processes exchanging at maximum one-photon can happen (i.e., $m = n \pm 1$). Notice that this is different from the standard perturbative expansion of the Peierls phase in the coupling strength, as the coefficients $g_{m,n}^{l,j}$ in Eq. (4) are non-linear functions of $\eta^{(r)}$. In fact, the virtual exchange of an arbitrary number of photons can still happen, as can be seen in, for example, the state-dependent frequency shift in the first line of Eq. (4). This truncation scheme is accurate in the high-frequency regime $\Omega \gg J', J$ discussed in this work, where the hybridization between bands with a different number of photons is small, but also in the presence of resonances involving one-photon exchange (see Methods).

High-frequency regime. To check the accuracy of this truncation scheme for a highly detuned cavity frequency, we plot in Fig. 1 a comparison between the exact spectrum of the system and the one obtained from the truncated Hamiltonian to one-photon processes, as a function of the coupling strength η (in units of J). It shows an excellent agreement for all values of the coupling and captures the cavity-induced localization (band collapse) at large values.

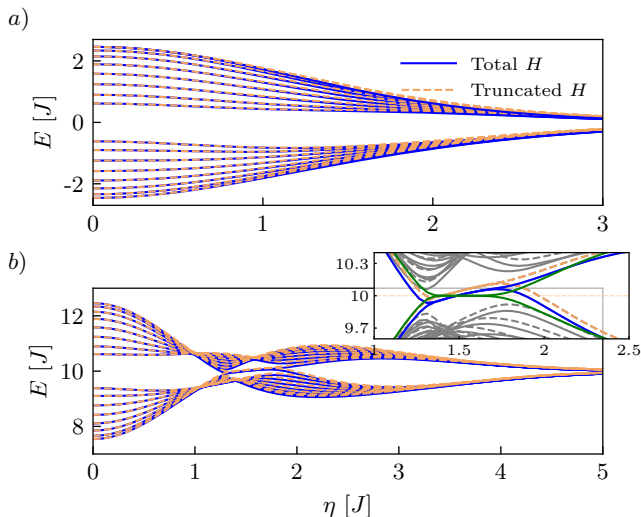


Figure 1. **Comparison between the energy spectrum of the full and the truncated Hamiltonian.** Comparison between the spectrum of the full and truncated Hamiltonians for the a) $n = 0$, and b) $n = 1$ subspaces. Inset: zoom into the edge states energy, where the spontaneous chiral symmetry breaking shifts them from the band center, and comparison with the mean-field spectrum (in green). Parameters: $J' = 1.5$, $J = 1$, $r' = 0.4$, $\Omega = 10$, $n_{\max} = 70$, $N = 16$.

Notice that the hopping amplitudes of the unperturbed SSH chain are chosen such that the system is topologically trivial for $\eta = 0$. This can be seen in Fig. 1, a) panel, where the subspace with $n = 0$ photons always lacks edge states. In contrast, the b) panel shows that in the subspace with $n = 1$ photons, topological edge states emerge upon increasing the interaction strength. This indicates that coupling a trivial SSH chain to a cavity can drive a topological phase transition, as it was the case in classical Floquet engineering [33]. However, given that each band renormalizes differently, they display topological phase transitions at different values of the coupling, depending on the number of photons involved. This provides an additional freedom to tune the system externally as compared to classical Floquet engineering, by modifying the number of photons in the cavity.

Despite this difference, classical and quantum Floquet engineering share certain similarities in the high-frequency regime. For example, the characteristic renormalization of the Floquet-Bloch bands in the classical case can be recovered from quantum Floquet engineering in the limit of $n \rightarrow \infty$ [16]. In the classical case, when different Floquet replicas are well-separated, one can describe the driven system using a stroboscopic Hamiltonian for the matter sector, captured by a Magnus expansion [34]. In the quantum case, for $\Omega \gg J, J'$, the number of photons n is a good quantum

number approximately, because transitions between different Fock states are very unlikely (which has indeed motivated the proposal of high-frequency expansions in the quantum regime as well [14, 16, 35]). Hence, one could think that as the bands are very weakly coupled for $\Omega \gg J, J'$, it would be possible to perform a mean-field (MF) analysis and obtain an effective matter Hamiltonian for each subspace, n , which characterizes the number of photons in the cavity.

This approach actually gives a good agreement with the bands renormalization of the exact spectrum (see Methods for an explicit comparison). However, there is a crucial detail in Fig. 1 which let us differentiate between the classical and quantum Floquet engineering, and it is directly linked with the existence of light-matter correlations.

In particular, Fig. 1 (inset) compares the spectrum of edge states for the exact and the truncated Hamiltonian (Eq. (4) with $m = n \pm 1$), with a MF description, which explicitly neglects correlations between both subsystems. (in Methods, we show the comparison for the full band). It shows that for the exact as well as for the truncated Hamiltonian, the edge states deviate from the center of the gap as a function of η , which means that chiral symmetry is spontaneously broken by light-matter interaction. However, in the MF approach, chiral symmetry is intact and the edge states remain pinned to zero energy. This can be confirmed by its impact on the topological invariant, which can be calculated for the interacting system (see Methods). The effect observed in the results for the exact and truncated hamiltonians is similar to that of long-range hopping in a generalized SSH model [36].

Let us compare this result with that of classical Floquet engineering. It is crucial to point out that, in the high-frequency regime, first-order corrections in the Magnus expansion [34] (which encode the exchange of virtual photons with the driving field) vanish for the SSH chain, and the driven system can be exactly described by the leading term, i.e., the time-averaged Hamiltonian. Therefore, chiral symmetry remains intact. In quantum Floquet engineering, quantum correlations induced by photon exchange are responsible for the spontaneous symmetry-breaking mechanism, even in the limit $\Omega \gg J, J'$, and neglecting them would incorrectly describe the system as chiral and with topologically protected edge modes.

In 2D classical Floquet systems, when a circularly polarized field is applied, Time Reversal Symmetry can be broken due to finite frequency corrections and the light polarization, changing the topology of the

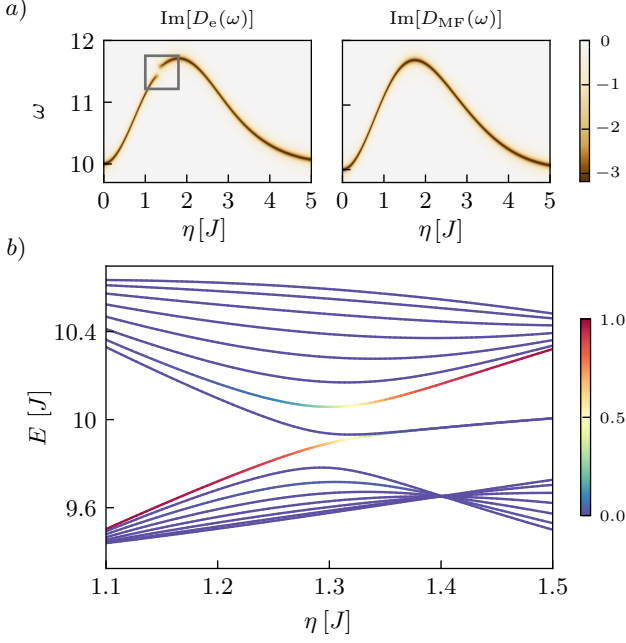


Figure 2. **Spectral signatures of light-matter correlations and dispersive shift of the cavity frequency** *a)* Spectral function for an empty cavity vs η for the MF solution D_{MF} , and the exact one including light-matter correlations D_e . The fermionic system is prepared in the ground state for a trivial chain. *b)* Spectrum of the subspace with $n = 1$ photons as a function of η . The color code indicates the effective cavity-mediated interaction strength \mathcal{P}_i , $r' = 0.4$, $\Omega = 10$, $n_{\text{max}} = 70$, $N = 16$. in *a)* $J' = 1.5$, $J = 1$.

system [37, 38]. However, this effect is still different from the quantum case, where the presence of light-matter correlations triggers a spontaneous symmetry-breaking mechanism.

Experimental signatures of light-matter correlations. Light-matter correlations are interesting from a fundamental perspective, but it is also important to relate them with experimental signatures. A well-known observable is the cavity frequency shift produced by the interaction with the quantum system. It is important for quantum technologies because it is proportional to the state of the fermionic system $\langle c_j^\dagger c_l \rangle$ and can be used to perform quantum non-demolition measurements [39–42]. Its value can be extracted from the photon spectral function $A(\omega) = -\frac{1}{\pi} \text{Im} \int dt e^{-i\omega t} D(t)$, with $D(t) = -i\theta(t) \langle [d(t), d^\dagger] \rangle$ the photonic Green’s function, and $A(\omega)$ can be experimentally measured by detection of the photons in the cavity. Now we describe how spectral features linked to light-matter correlations encode information about the topology of the quantum system. Let us first consider the cavity in its vacuum state $n = 0$ and, to isolate the role of light-matter correlations, compare the MF result with the one including light-matter

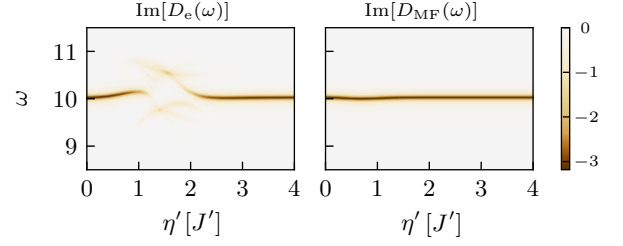


Figure 3. **Spectral photonic function when an edge state is occupied.** Spectral function for an empty cavity vs η' for the MF solution D_{MF} and the exact one including light-matter correlations D_e . The fermionic system is prepared in the edge state for a topological chain, $r' = 0.4$, $\Omega = 10$, $n_{\text{max}} = 70$, $N = 16$, $J' = 1$, $J = 1.5$.

correlations. Fig. 2 *a)* shows that, for the fermionic system in its ground state, MF correctly captures the cavity frequency shift (details of the calculation in the SM):

$$\delta\Omega = \sum_{j,l} J_{j,l} e^{-\eta_{l,j}^2/2} \langle c_j^\dagger c_l \rangle, \quad (5)$$

but fails to describe the fine spectral details near $\eta \sim 1.3$, which are originated by light-matter correlations (framed region in the left plot). The important effect of correlations at this point is related to the presence of topological edge states in subspaces with additional photons and their different coupling to the photonic field.

This mechanism is illustrated in Fig. 2 *b)*, which shows the spectral flow in the $n = 1$ subspace, as the light-matter coupling increases. The color code indicates the effective cavity-mediated interaction between the ground state of the total system, $|\Psi_{\text{g.s.}}\rangle$, and the i^{th} state in the $n = 1$ subspace, $|\Psi_i^{(1)}\rangle$ ($i = 1, \dots, 2N$), calculated as $\mathcal{P}_i = \langle \Psi_0 | d | \Psi_i^{(1)} \rangle \langle \Psi_i^{(1)} | d^\dagger | \psi_0 \rangle$. Fig. 2 *b)* shows that, initially, the interaction with the $n = 1$ subspace is mainly with the state on top of the valence band. However, this state becomes an edge state near $\eta \sim 1.3$, and since the edge states are exponentially decoupled from the bulk [43], the interaction jumps to the state at the bottom of the conduction band, producing the correction to the MF result.

Importantly, if the fermionic system initially is in the topological phase for $\eta = 0$, the relation between the topological phase transition in the upper photonic band and the corrections to $A(\omega)$ due to light-matter correlations still holds. Thus, it does not depend on the initial state of the system.

Strikingly, the effect is even stronger if the system is not in its ground state but in an edge state. In Fig. 3 we consider that the chain has non-trivial topology for $\eta' = 0$ (in units of $J' = 1$). Then, as the edge states are exponentially decoupled from the bulk, the cavity frequency does not shift. However, when the edge states

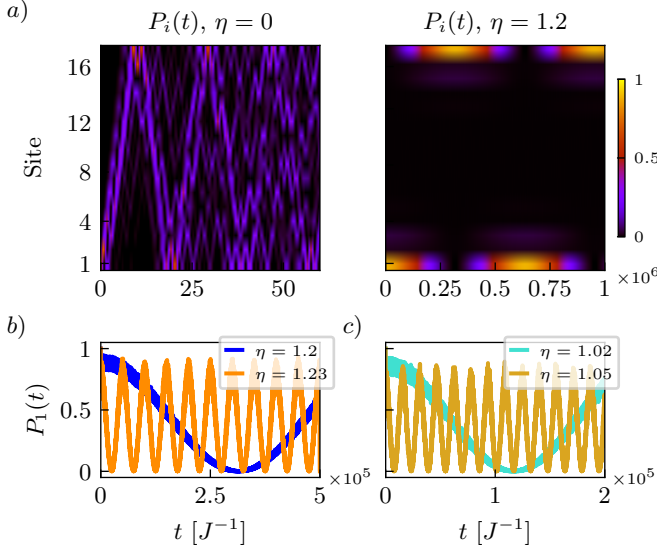


Figure 4. Charge dynamics in the interacting system. *a)* Fermionic occupation probability $P_i(t)$ of each site of the chain $i = 1, \dots, 2N$ as a function of time, for a particle initially occupying the first site, and $n = 2$ photons. For $\eta' = 0$ the system lacks edge states and the particle propagates freely. In contrast, for $\eta = 1.2$ the system has edge states and the particle oscillates between ending sites. *b)* Fermionic occupation probability of the first site $P_1(t)$, as a function of time, for different η and $n = 2$, showing that the coupling can be used to control the oscillation frequency. *c)* Same as in panel *b)*, with $n = 3$, showing that changing the number of photons also can control the oscillation frequency, $J' = 1.5$, $J = 1$, $r' = 0.4$, $N = 16$, $\Omega = 10$, $n_{\max} = 50$.

in the $n = 1$ merge with the bulk, correlations strongly affect the MF value of $A(\omega)$, until the $n = 1$ band becomes topological again. This means that we can use the cavity, not only to induce a topological phase transition but also its spectral function to indirectly detect the presence of topological transitions in subspaces with a different number of photons.

State transfer dynamics. As we discussed above, in the absence of chiral symmetry, the edge states in the SSH chain loose their topological protection, but this does not mean that they cannot be used for practical applications. It has been proposed that, as they are exponentially localized states, their small overlap between the two ends of the chain can be used in quantum state transfer [44–47].

Now we show that in Quantum Floquet Engineering, the cavity can be used to control the transfer dynamics. On the one hand, we have shown that edge states can be created in a trivial chain, if it is coupled to a cavity with $n > 0$. This would allow to implement state transfer protocols in systems that originally lack edge states. On the other hand, it provides a way to tune the

Hamiltonian, and then the transfer time between the two ends of the chain.

The first case is shown in the left panel of Fig. 4 *a)*, where a particle initially at site 1 of an SSH chain in the trivial topological phase, freely evolves populating all sites of the chain. In contrast, the right panel shows that if the chain is coupled to a cavity with $n = 2$ photons, there are coherent oscillations between the two ends, confirming the presence of cavity-induced edge states. Importantly, its dynamics confirms that, although chiral symmetry is broken, the transfer between the two ends of the chain still is efficient.

For the second case, we can manipulate the transfer dynamics in two ways: by modifying the light-matter coupling, for example by tuning the frequency of the cavity [48] or by changing the number of photons. This is shown in panels *b)* and *c)* of Fig. 4, respectively. For the second case, we have used the fact that the subspace with $n = 3$ photons is also topological for certain values of η .

Conclusions. We have shown that Quantum Floquet Engineering is much more complex than its classical counterpart, even in the case of large cavity frequency, where one expects that the cavity photons can be easily traced-out and light-matter correlations neglected, without relevant consequences. While the connection between the classical and quantum case has been explored before [15, 16], the role of quantum correlations has been so far neglected. To explore this, we have developed a non-perturbative truncation method that allows us to reduce the highly non-linear gauge-invariant Hamiltonian, describing a chain coupled to a cavity, to a simpler one that remains valid for arbitrary light-matter coupling.

As a particular case, we have considered a SSH chain and have shown that the interaction with the cavity can drive a topological phase transition from a trivial to a topological phase. Importantly, this transition can be controlled via the number of photons in the cavity, which is a tuning parameter absent in classical Floquet engineering.

We have found that in contrast with classical Floquet engineering [33], where the coupling to light conserves the symmetries of the system, in Quantum Floquet engineering light-matter correlations can spontaneously break chiral symmetry, even in the high frequency regime, affecting the topological protection of the edge states.

In addition, we have found that light-matter correlations can be experimentally detected in the photon spectral function, and that they contain information about the cavity-induced topological phase transitions in the system. This is a consequence of the different response of bulk and edge states to the presence of cavity photons. Finally, we have shown that the cavity also provides us

with a way to control the state transfer between edges of the chain. It can be used to create or destroy the edge states, as well as to tune the transfer time between the two sides.

Acknowledgments G.P. and B.P.G. acknowledge the Spanish Ministry of Economy and Competitiveness for financial support through the grant: PID2020-117787GB-I00. A.G.L acknowledges support from the European Union's Horizon 2020 research and innovation program under Grant Agreement No. 899354 (SuperQuLAN). All the authors also acknowledge support from CSIC Interdisciplinary Thematic Platform (PTI+) on Quantum Technologies (PTI-QTEP+).

Methods

Light-matter coupling in the Coulomb and dipole gauge. The starting point is the tight-binding Hamiltonian $H_{\text{el}} = \sum_{ij} J_{ij} c_i^\dagger c_j$ that is coupling to a single-mode photonic field $H_{\text{phot}} = \Omega d^\dagger d$. In general, the minimal-coupling Hamiltonian describing the light-matter interaction in the Coulomb gauge can be implemented through an unitary transformation U acting on the fermionic degrees of freedom only [21, 24, 30], with

$$U = \exp \left\{ i(d^\dagger + d) \sum_{ij} \chi_{ij} c_i^\dagger c_j \right\} \quad (6)$$

where $\chi_{ij} = \langle i | \chi | j \rangle = \int d\vec{r} \phi_i^*(\vec{r}) \chi(\vec{r}) \phi_j(\vec{r})$, being $\phi_i(\vec{r})$ the single-particle wavefunctions localized around each lattice site i , and $\chi(\vec{r})$ chosen such that $\nabla \chi(\vec{r}) = e A_0(\vec{r})$, or equivalently,

$$\chi(\vec{r}) = e \int_{\vec{r}_0}^{\vec{r}} A_0(\vec{r}') \cdot d\vec{r}' \quad (7)$$

In general, the vector potential in a 1D system can be written as $\vec{A}(r) = A_0(r)(d^\dagger + d)\hat{u}(r)$. Under the dipole approximation used in the main text $A_0(r) \approx A_0$, and assuming that the vector potential is orientated along the axis of the electronic chain (without loss of generality, we will assume this is the x axis), this expression can be further simplified to yield $\chi(r) = e A_0 r$, where we have dropped the vectorial notation for the position coordinate (we have also taken $r_0 = 0$). Therefore, we can also write $\chi_{ij} \approx \delta_{ij} \chi_{ii} = e A_0 r_i \delta_{ij}$, and the final form of the transformation U is

$$U = \exp \left\{ i e A_0 (d^\dagger + d) \sum_i r_i c_i^\dagger c_i \right\} \quad (8)$$

Using the Baker-Campbell-Hausdorff formula, the transformed fermionic operators will then give

$$U^\dagger c_i U = c_i e^{i e A_0 r_i (d^\dagger + d)}, \quad U^\dagger c_i^\dagger U = c_i^\dagger e^{-i e A_0 r_i (d^\dagger + d)} \quad (9)$$

The Peierls Hamiltonian H shown in Eq. 1 in the main text can be obtained by operating $H_{\text{PS}} = H_\Omega + U^\dagger H_{\text{el}} U$.

In conclusion, the Peierls substitution yields a minimal-coupling Hamiltonian under the dipole approximation, satisfying the gauge principle. Note that further orbital structure $c_i^{(\dagger)} \rightarrow c_{i\mu}^{(\dagger)}$ has not been taken into account, in which case there would be additional dipole-like terms connecting different orbitals. In general, without applying the dipole approximation and including a nontrivial structure in both real and orbital space, the transformation of the fermionic operators would give

$$U^\dagger c_i U = \exp \left\{ i(d^\dagger + d) \sum_{ij, \mu\mu'} \chi_{ij}^{\mu\mu'} c_{i\mu}^\dagger c_{j\mu'} \right\} \quad (10)$$

The results of this section, and in particular Eqs. 6 and 7, are also in agreement with the parallel transporter introduced in [23] to derive gauge-invariant Hamiltonians using lattice gauge theory for two-level systems, and with the results obtained for the Dicke and Hopfield models in [24].

An alternative form of the light-matter coupling can be obtained by writing the Peierls Hamiltonian in the dipole gauge (DG). This transformation, that we will denote T , is the inverse of U

$$T = U^\dagger, \quad T = \exp \left\{ -i e A_0 (d^\dagger + d) \sum_i r_i c_i^\dagger c_i \right\} \quad (11)$$

and is applied only on the photonic operators, $H_{\text{DG}} = T^\dagger H_\Omega T + H_{\text{el}}$. In particular, the transformed photonic operators give

$$T^\dagger d T = d + i \sum_j r_j c_j^\dagger c_j, \quad T^\dagger d^\dagger T = d^\dagger - i \sum_i r_i c_i^\dagger c_i \quad (12)$$

and H_{DG} has the following form

$$H_{\text{DG}} = \Omega d^\dagger d + H_{\text{el}} + i e A_0 \Omega (d - d^\dagger) \sum_i r_i c_i^\dagger c_i \quad (13) \\ + e A_0 \Omega \left(\sum_i r_i c_i^\dagger c_i \right)^2$$

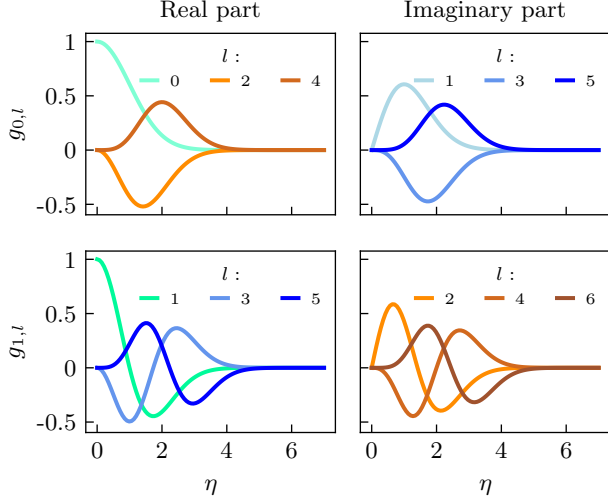


Figure 5. **Coefficients g_{sl} as a function of η for different values of s, l .** When $s = l$, the Laguerre polynomials are obtained.

While gauge invariance ensures that the physical results are independent of the choice of gauge, the form of the light-matter coupling is gauge dependent. In the previous expression, the interaction with photons in the cavity shifts the energy of each site of the chain (last term in first line) through the action of the displacement field $\Pi \propto i(d - d^\dagger)$. An additional photon-assisted density interaction term (second line) that affects only the electronic subsystem must be included to keep gauge invariance for arbitrary coupling strength [49]. While this term can be neglected for the case of a single-occupied electronic system, the local contribution $eA_0\Omega \sum_i r_i^2 c_i^\dagger c_i$ must be kept.

Derivation of the Peierls Hamiltonian in the basis of photon states. In this section, we detail the derivation of the Peierls Hamiltonian in the photon basis. We first apply the Baker-Hausdorff-Campbell identity for non-commuting operators A and B : $e^{A+B} = e^{-[A,B]/2}e^Ae^B$, to the Peierls operator:

$$e^{i\eta_{ji}(d^\dagger+d)} = e^{-\eta_{ji}^2/2} e^{i\eta_{ji}d^\dagger} e^{i\eta_{ji}d}, \quad (14)$$

This allows us to factor and re-organize the different powers of the creation and annihilation operators, which now are weighted by an additional exponential pre-factor $e^{-\eta_{ji}^2/2}$. Applied on the photonic number state $|n\rangle$, one gets

$$e^{i\eta_{ji}(d^\dagger+d)}|n\rangle = e^{-\eta_{ji}^2/2} \sum_{q,k=0} \Theta(q,n,k)|n-k+q\rangle \quad (15)$$

where we have defined

$$\Theta(q,n,k) = \frac{(i\eta)^{q+k} \sqrt{(n-k+q)!n!}}{q!k!(n-k)!} \quad (16)$$

where we have used the definitions of the creation/annihilation operators $d|n\rangle = \sqrt{n}|n-1\rangle$ and $d^\dagger|n\rangle = \sqrt{n+1}|n+1\rangle$. Then, for any two given photonic subspaces l and s , the prefactors g_{ls}^{ji} are:

$$g_{ls}^{ji} = \langle l|e^{i\eta_{ji}(d^\dagger+d)}|s\rangle = e^{-\eta_{ji}^2/2} \sum_{q=0}^{\infty} \sum_{k=0}^s \frac{(i\eta_{ji})^{q+k}}{q!k!(s-k)!} \sqrt{l!s!} \quad (17)$$

For $l = s$ (diagonal terms), this finite sum converges to the Laguerre polynomials L_s , and the off-diagonal terms are proportional to the Kummer's confluent hypergeometric function ${}_1F_1(s,l,\eta^2)$, as shown in the main text.

We now plot the analytical solution for the coefficients $g_{nn} = e^{-\eta^2/2} L_n(\eta^2)$ and $g_{mn} = e^{-\eta_{ji}^2/2} \frac{(i\eta)^{n-m}}{(n-m)!} \sqrt{\frac{n!}{m!}} {}_1F_1(m,n,\eta^2)$ as a function of the coupling (see Fig. 5).

While the Laguerre polynomials are purely real, the coefficients g_{mn} are real or imaginary depending on the values for n and m . This is shown in Fig. 5, where only the non-zero contribution has been plotted for each n, m .

Importantly, in the non-interacting limit $\eta \rightarrow 0$, the diagonal coefficients $g_{nn} \rightarrow 1$ go to one, while the off-diagonal ones $g_{mn} \rightarrow 0$: one-photon transitions disappear and we are left with the free fermionic Hamiltonian, as expected.

The oscillating behaviour of both g_{nn} and g_{mn} indicates the dominant subspaces will depend on the coupling strength considered, with a highly non-linear dependence.

Lastly, the dynamical localization prefactor $\exp(-\eta^2/2)$ ensures that all coefficients go to zero for large enough coupling strength, for all n, m .

SSH Hamiltonian. The SSH model is a tight-binding model describing non-interacting electrons in a 1D lattice with an alternating pattern of first-neighbour hoppings, J' and J . This dimerized structure motivates the definition of two sublattices, A and B , and the use of sublattice creation/annihilation operators, $a_\alpha^{(\dagger)}$ and $b_\alpha^{(\dagger)}$, where $\alpha = 1, 2, \dots, N$ is a cell index and N is the total number of cells/dimers. Its second-quantization Hamiltonian can be written as

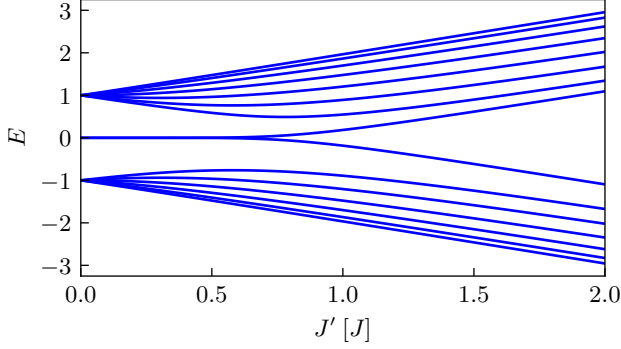


Figure 6. **Energy spectrum of the SSH model.** The value of $J = 1$ is fixed. In the left side of the plot ($J' < J$), the presence of in-gap edge states indicates that the system has non-trivial topology.

$$H_{\text{SSH}} = \sum_{\alpha}^N (J' a_{\alpha}^{\dagger} b_{\alpha} + J b_{\alpha}^{\dagger} a_{\alpha+1}) + \text{h.c.} \quad (18)$$

Notice that the hopping J' takes place within the same dimer, and that is why it is usually referred to as the intra-dimer hopping, while J is the inter-dimer hopping, connecting sites belonging to different dimers. Fig. 6 shows the energy spectrum as a function of the hopping amplitude J' , for a fixed $J = 1$. For $J' < J$, the presence of in-gap topological edge states denotes that the chain has non-trivial topology.

Truncated Hamiltonian for low-photon frequency and comparison with the Taylor-expanded Hamiltonian. The total Hamiltonian in Eq. (4) still is exact, and contains all orders of the vector potential, which are essential for maintaining gauge invariance for arbitrary coupling strength. In contrast, a naive Taylor expansion of the Peierls operator with the usual paramagnetic $\propto (d^{\dagger} + d)$ and diamagnetic $\propto (d^{\dagger} + d)^2$ terms would fail as the coupling strength increases towards the ultrastrong coupling regime [16, 50, 51]. The difference lies in the coefficients $g_{m,n}^{l,j}$, which are non-linear functions of $\eta_{l,j}$, and therefore the expansion in photonic Hubbard operators is unequivocal to that of a direct series expansion in powers of $\eta_{l,j}$.

Fig. 7a) shows the energy spectrum for truncated Peierls Hamiltonian and the Taylor-expanded Hamiltonian to second order,

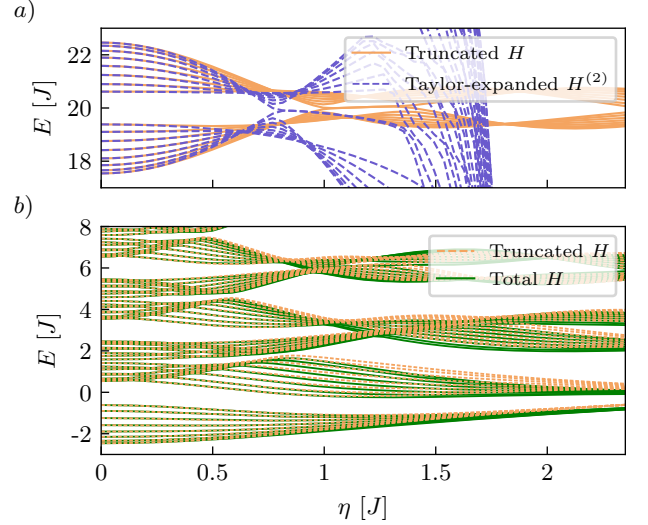


Figure 7. **Energy spectrum for the interacting systems under different regimes of parameters and approximations.** a) Comparison of the energy spectrum of the truncated Hamiltonian and $H^{(2)}$, for $\Omega = 10$, as a function of the coupling strength. b) Comparison of the energy spectrum of the total Hamiltonian and the truncated one including only one-photon transitions, for a photon frequency lower than the bandwidth of the chain, $\Omega = 3$, $J' = 1.5$, $J = 1$, $r' = 0.4$, $n_{\text{max}} = 80$, $N = 16$.

$$H^{(2)} = \sum_{\langle l,j \rangle} \left[J_{l,j} - \frac{\eta_{j,l}^2}{2} (d^{\dagger} + d)^2 \right] c_l^{\dagger} c_j + i(d^{\dagger} + d)\mathcal{J} \quad (19)$$

where $\mathcal{J} = \sum_{\langle l,j \rangle} \eta_{j,l} J_{l,j} (c_j^{\dagger} c_l - c_l^{\dagger} c_j)$ contains a photon-dependent correction term to the hopping amplitudes. $H^{(2)}$ shows a good agreement for small coupling strength but differs radically from the Peierls Hamiltonian as the coupling increases. This is a consequence of the violation of gauge invariance. Accuracy would improve as higher orders of the photonic field are included.

Now, we test the validity of the truncated Hamiltonian far from the high frequency regime, when Ω is of the same order of magnitude as the fermionic bandwidth. Hence, mixed photonic bands are expected to appear in the energy spectrum, and the effect of higher photon transitions cannot be neglected for arbitrary coupling.

Fig. 7b) shows the energy spectrum of the total H and truncated one, for $\Omega = 3$ and a bandwidth of $\Delta = 5$. There is an overlap between different photonic bands, which becomes evident as the coupling is increased, resulting in a pattern of resonances and anticrossings.

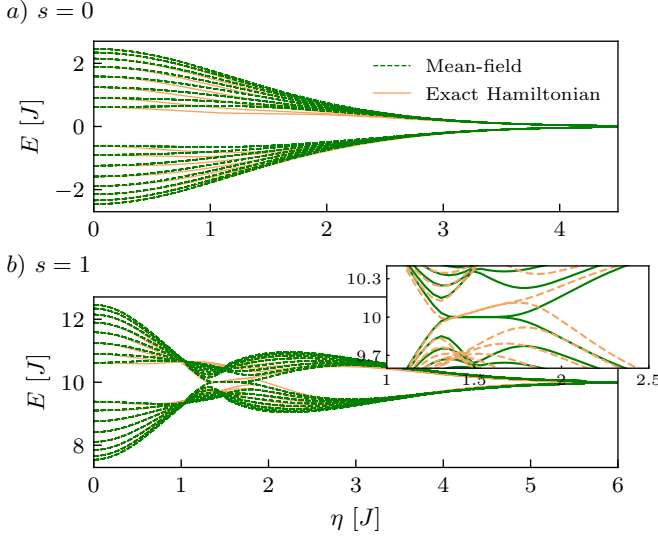


Figure 8. **Comparison between the energy spectrum of the truncated Hamiltonian and the mean-field approach.** Comparison between the exact truncated (orange) and the mean-field fermionic Hamiltonian (purple) as a function of the coupling strength η' , for different photonic bands: **a)** $s = 0$, and **b)** $s = 2$. The grey, dashed lines correspond to the center of the band at $\eta' = 0$. In **a)**, the inset shows the renormalized hopping amplitudes $\tilde{t}^{(l)}$ vs. η' . In **b)**, the first inset shows the energy of the edge states vs. η' , highlighting the difference between the chiral-symmetric MF spectrum and the exact truncated one in which chiral symmetry is broken. The second inset shows the hopping renormalization, with the same color code as in **a)**, $t' = 1.5$, $t = 1$, $N = 8$ unit cells, $n_{\max} = 50$, $\Omega = 10$, $r' = 0.4$.

The truncated Hamiltonian reproduces the result of H for small coupling strength with high accuracy, but as η' becomes larger, higher photon transitions are activated. Then, when the coupling becomes the dominant energy scale, both the exact and the truncated Hamiltonians yield the same result, as expected.

Mean-field Hamiltonian. We have shown that a simplified version of the gauge invariant Hamiltonian in the Coulomb gauge can be obtained by using disentangling techniques and truncating to one-photon processes. Now, we explore which features of the energy spectrum are retained when an even simpler approximation is used, i.e., a mean-field decoupling scheme in which each operator is rewritten as $\mathcal{O} = \langle \mathcal{O} \rangle + \delta\mathcal{O}$, separating its mean value $\langle \mathcal{O} \rangle$ from the contribution of quantum fluctuations $\delta\mathcal{O}$. At the MF level (linear terms in $\delta\mathcal{O}$), we obtain two effectively decoupled Hamiltonians for each subsystem, where the back-action due to the interaction is encoded in renormalized system parameters. An additional fluctuations Hamiltonian (second-order in $\delta\mathcal{O}$) encodes the role of quantum fluctuations, introducing

correlations between subsystems. A MF analysis of the problem allows to identify which features are captured by the photo-dressing of the fermionic system and which of them are linked to electron-photon correlations. In the following, the MF approach will be used on the truncated version of the exact Hamiltonian.

For the photonic field, the MF decoupling on the truncated Hamiltonian gives a particularly simple description: the resulting Hamiltonian is diagonal in the basis of Hubbard operators Y^{nn} . First, let us define the following fermionic operators, which contain the energy contribution of both the inter- and intra-dimer hopping

$$f'_+ = t' \sum_{\alpha} a_{\alpha}^{\dagger} b_{\alpha} = (f'_-)^{\dagger}, \quad f_+ = t \sum_{\alpha} b_{\alpha}^{\dagger} a_{\alpha+1} = (f_-)^{\dagger}, \quad (20)$$

together with $f^{(l)} = f_+^{(l)} + f_-^{(l)}$. Then, the MF photonic Hamiltonian can be readily written as

$$H_{\text{MF,phot}} = \sum_n \left\{ n\Omega + \langle f' \rangle g'_{nn} + \langle f \rangle g_{nn} \right\} Y^{nn}. \quad (21)$$

Note that one-photon transitions are absent in the MF photonic Hamiltonian $H_{\text{MF,phot}}$, which is diagonal in the photonic operators. This is due to the symmetry of the truncated Peierls operator in Eq. (2) and the form of the off-diagonal coefficients $g_{n,n+1}^{(l),\pm}$. In general, the creation/annihilation of m photons in the system through the operators $Y^{n+m,n}/Y^{n,n+m}$ is linked to the electronic inter- and intra-dimer hopping, where the corresponding tunneling amplitudes are weighted by the prefactors $g_{n,n+m}^{(l),\pm}$. For the case of one-photon transitions, the direction of the hopping (to the left, $\eta^{(l)} > 0$, or to the right, $\eta^{(l)} < 0$) has the effect of adding an extra sign to $g_{n,n+1}^{(l),\pm}$, so that they finally cancel out in $H_{\text{MF,phot}}$. Note that for arbitrary m , all odd-photon transitions ($m = 1, 3, 5, \dots$) would be absent from the MF Hamiltonian, while even ones ($m = 2, 4, 6, \dots$) are not cancelled out. This is agreement with Ref. [12].

Then, the eigenstates of $H_{\text{MF,phot}}$ in Eq. (21) can be labelled with the photon number $n = 0, 1, 2, \dots$, being $n = 0$ the ground state with zero photons. This means that the different photonic subspaces will not hybridize for large coupling strength, and the number of photons in the system is constant in time.

The Hamiltonian in Eq. (21) indicates that the interaction with the fermionic system shifts the energy of the cavity photons, which depends on the fermionic state through $\langle f^{(l)} \rangle = \text{Tr}\{\rho_{\text{MF,fer}} f^{(l)}\}$. Being absent in the

classical regime, the frequency shift is crucial in cavity QED set-ups for quantum non-demolition measurements on the fermionic system using the photonic radiated signal [52–55].

For the fermionic system, the MF decoupling yields an unperturbed SSH Hamiltonian with renormalized hopping amplitudes due to the interaction with the photonic field,

$$t^{(\prime)} \rightarrow \tilde{t}^{(\prime)} = t^{(\prime)} g_{s,s}^{(\prime)} = t^{(\prime)} e^{-\eta^{(\prime)2}/2} L_s \left(\eta^{(\prime)2} \right). \quad (22)$$

Note that both \tilde{t}' and \tilde{t} inherit the dynamical localization prefactors that ensures the suppression of the hopping at large coupling strength, while the dependence on the Laguerre polynomial $L_s(\eta^{(\prime)2})$ gives an oscillatory dependence with η' . Here we have assumed that the cavity is prepared with a fixed number of photons, $\rho_{\text{MF,phot}} = |s\rangle\langle s|$.

Fig. 8 shows the MF fermionic energy spectrum compared with the exact truncated Hamiltonian. The former reproduces the topological phase transitions as a function of the coupling strength, which indicates that topology is controlled by the dressing of the fermionic degrees of freedom (first term in Eq. (4)) and the ratio of the renormalized hoppings \tilde{t}'/\tilde{t} .

Calculation of the topological invariant for the interacting system. The fermionic Green's function (GF) can be used to characterize the topological properties of many-body system [56–60]. In particular, for one-dimensional systems displaying chiral symmetry, the topological invariant can be computed from [57]

$$\mathcal{W} = \frac{1}{4\pi i} \int_{-\pi}^{\pi} dk \Sigma [G(k, \omega = 0)]^{-1} \partial_k G(k, \omega = 0), \quad (23)$$

where $\Sigma = \sigma_z$ represents chiral symmetry, with $\Sigma^2 = 1$. This expression is valid for both non-interacting and interacting systems, and in the former case, it can be reduced to the well-known expression of the topological invariant for one-dimensional [61].

For a SSH chain interacting with the photonic field, we can define the mixed GF as

$$G_{\alpha,\beta}^{s,s}(\omega, k) = \langle \langle \alpha_k Y^{s,s}; \beta_k^\dagger \rangle \rangle, \quad (24)$$

where s represents a fixed number of photons in the system and $\alpha, \beta = A, B$ account for the sublattices of the chain, together with the completeness relation

$G_{\alpha,\beta}(\omega, k) = \langle \langle \alpha_k; \beta_k^\dagger \rangle \rangle = \sum_n G_{\alpha,\beta}^{n,n}(\omega, k)$. Since it contains both fermionic and photonic operators, $G_{\alpha,\beta}^{s,s}(k, \omega)$ has information about the correlations between both subsystems.

For $\eta' = 0$, the distinct photonic subspaces are decoupled, and the energy spectrum consists on infinitely many photonic bands (bounded from below) of the electronic band structure, separated by an energy splitting of Ω . Each of them have a well-defined photon number. Then, the eigenstates $|\Psi(k)\rangle$ of the total Hamiltonian can be factorized between a fermionic part $|\psi(k)\rangle$ and a photonic one given by $|s\rangle$, where s is the number of photons, namely $|\Psi(k)\rangle = |\psi(k)\rangle \otimes |s\rangle$. Therefore, in this limit, only the eigenstates $|\Psi_i\rangle$ with $s_i = s$ photons would give a non-zero contribution to $G_{\alpha,\beta}^{s,s}(\omega, k)$, thus recovering the expected result for the non-interacting system. For each photonic band, the associated topological invariant \mathcal{W}_s would be defined by the ratio between the bare hopping amplitudes.

As the coupling is increased, the eigenstates acquire a non-zero weight on different photonic subspaces, and hence $|\Psi(k)\rangle \neq |\psi(k)\rangle \otimes |s\rangle$. This hybridization of the different photonic subspaces caused by the terms $\propto (Y^{n,n+1} + Y^{n+1,n})$ in the Hamiltonian, is responsible for the spontaneous breaking of chiral symmetry and can be expected to be detected in $G_{\alpha,\beta}^{s,s}(\omega, k)$ as well. How this affects the topological properties of each band can be quantized through the calculation of the corresponding topological invariant \mathcal{W}_s ,

$$\mathcal{W}_s = \frac{1}{4\pi i} \int_{-\pi}^{\pi} dk \Sigma [G^{s,s}(k, \omega = 0)]^{-1} \partial_k G^{s,s}(k, \omega = 0). \quad (25)$$

In conclusion, the changes in \mathcal{W}_s induced by the interaction can be directly linked to the hybridization between different bands, and therefore provide a quantitative measure of the breaking of chiral symmetry in the system.

To evaluate Eq. (25), one needs to calculate the mixed GF $G^{s,s}(k, \omega)$. On the one hand, it can be obtained numerically; on the other hand, an analytical solution for $G_{\alpha,\beta}^{s,s}(\omega, k)$ can be found by writing their equation of motion (EOM) in time domain

$$i \frac{dG_{\alpha,\beta}^{s,s}(k, t)}{dt} = \delta(t) \left\{ \alpha_k Y^{s,s}(t), \beta_k^\dagger \right\} - i\theta(t) \langle \left\{ \left[\alpha_k^\dagger Y^{s,s}, \mathcal{H}(k) \right], \beta_k^\dagger \right\} \rangle. \quad (26)$$

Solving Eq. (26) including one-photon transitions is more challenging, and requires to define additional GFs

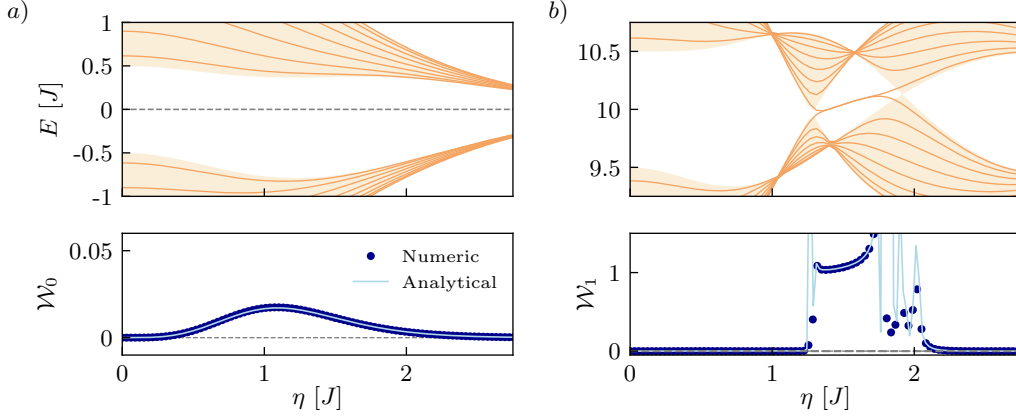


Figure 9. **Topological invariant for the interacting system.** These plots reflect the loss of chiral symmetry due to electron-photon correlations, as reflected in the energy spectrum and the topological invariant of each photonic band: *a*) $n = 0$, and *b*) $n = 1$. The shaded regions in the top plots indicate the width of the corresponding energy band in the thermodynamic limit, $J' = 1.5$, $J = 1$, $r' = 0.4$, $n_{\max} = 80$, $N = 16$.

with their corresponding EOMs, so that one is finally left with a system of coupled differential equations. In practice, solving this exactly is not usually tractable, and one has to consider a decoupling scheme that allows to close the system of EOMs.

First, we have considered single occupation for the SSH chain, which greatly simplifies the fermionic algebra. Second, with the truncation of $\mathcal{H}(k)$, the EOM can be restricted to those terms involving only one-photon transitions, namely $G_{\alpha,\beta}^{s\pm 1,s}(k,\omega)$ and $G_{\alpha,\beta}^{s,s\pm 1}(k,\omega)$. This entails a major reduction of the equations and enables the solution of the system, that would otherwise involve infinitely many GFs of the form $G_{\alpha,\beta}^{n,n+l}$ and $G_{\alpha,\beta}^{n+l,n}$ ($l = 1, 2, \dots$). With all this, and neglecting off-diagonal couplings, the solution for $G_{\alpha,\beta}^{s,s}(k,\omega)$ can be written in the form

$$G^{s,s}(k,\omega) = \frac{\langle Y^{s,s} \rangle}{2\pi} [F^{s,s}(k,\omega)]^{-1}, \quad (27)$$

where $F^{s,s}$ is a 2×2 matrix which contains the pole structure for $G^{s,s}(k,\omega)$. By defining $\varepsilon_{O,s}(k) = h_{O,s}(k)h_{O,s}^*(k)$, we can write the following expression for the matrix elements of $F^{s,s}$,

$$F_{A,A}^{s,s}(k,\omega) = \omega - \frac{\varepsilon_{O,s}(k)[\omega + \Omega]}{p_{s+1}^+(\omega,k)} - \frac{\varepsilon_{O,s-1}(k)[\omega - \Omega]}{p_{s-1}^-(\omega,k)}, \quad (28)$$

$$F_{A,B}^{s,s}(k,\omega) = -h_{D,s}(k) - \frac{h_{O,s}^2(k)h_{D,s+1}^*(k)}{p_{s+1}^+(\omega,k)} - \frac{h_{O,s-1}^2(k)h_{D,s-1}^*(k)}{p_{s-1}^-(\omega,k)}, \quad (29)$$

$$F_{B,A}^{s,s}(k,\omega) = [F_{A,B}^{s,s}(k,\omega)]^*, \quad F_{B,B}^{s,s}(k,\omega) = F_{A,A}^{s,s}(k,\omega), \quad (30)$$

with $p_s^+(k,\omega) = (\omega + \Omega)^2 - \varepsilon_{D,s}(k)$ and $p_s^-(k,\omega) = (\omega - \Omega)^2 - \varepsilon_{D,s}(k)$.

The first term in Eqs. (28) and (29) accounts for the mean-field result of dressed electrons, while the second and third terms contain the contribution of one-photon transitions, which allows us to interpret the implications for the topology of fermionic chain. Note that those terms contain additional poles with mixed light-matter resonances, due to the presence of correlations between subsystems.

Physically, the additional terms in $F_{\alpha,\alpha}^{s,s}(k,\omega)$ indicate the transfer of spectral weight to the subspaces of $(s+1)$ - (second term in Eq. (28) and $(s-1)$ -photons (third term in Eq. (28)). Interestingly, since $\varepsilon_s^2(k) \neq \varepsilon_{s-1}^2(k)$, the transfer of spectral weight is not symmetric. Therefore, the exchange of one-photon from a given photonic band with the upper/lower bands are not equivalent.

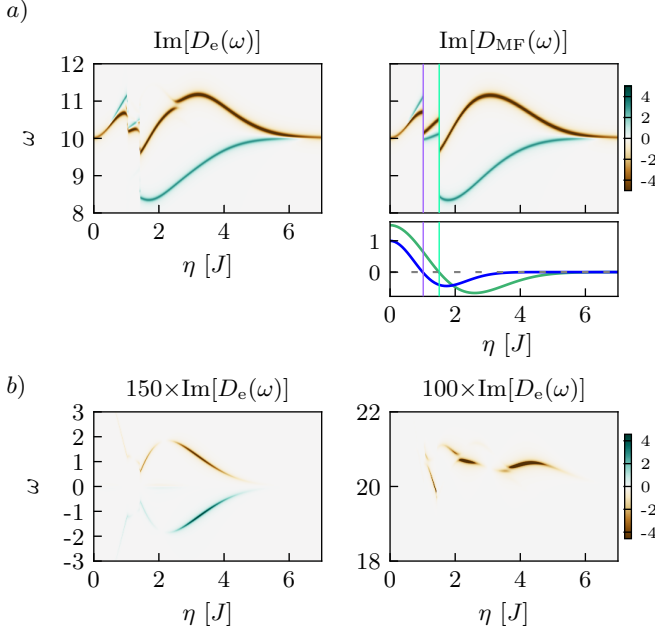


Figure 10. **Spectral function for a non-empty cavity.** $D_{MF(\omega)}$ and $D_{e(\omega)}$ for $n = 1$ as a function of η and ω . The fermionic system is prepared in the ground state for a trivial chain. Panel a) shows the renormalization of the cavity frequency and the appearance of additional excitations, while the bottom panel indicates the connection between the abrupt changes in the poles and the hopping renormalization. Panel b) shows additional light-matter resonances that appear in D_e and that are absent in the MF solution, $J' = 1.5$, $J = 1$, $r' = 0.4$, $\Omega = 10$, $n_{\max} = 70$, $N = 16$.

Fig. 9 shows the energy spectrum and corresponding topological invariant for the a) zeroth photonic band, and b) first photonic band. The top panels show the detail of the asymmetry induced by the coupling with the cavity photons. This is specially relevant for the topological edge states in d), since the breaking of chiral symmetry destroys topological protection. Importantly, both \mathcal{W}_0 and \mathcal{W}_1 capture the breaking of chiral symmetry through the loss of quantization. Note how the asymmetry in the spectrum is proportional to the deviations in the topological invariant in both cases. This is specially evident in panel a), where the maximum asymmetry corresponds to the maximum value of \mathcal{W}_0 . Similarly, in the topological region of the b), \mathcal{W}_1 takes the closest values to 1 when the deviation of the energy.

Spectral function for a non-empty cavity. Let us now consider a different state preparation with a non-empty cavity, with $n = 1$ photons, which is depicted in Fig. 10. Panel a) shows the comparison between the MF and the exact result, $D_{MF}(\omega)$ and $D_e(\omega)$, respectively. While the photon frequency is shifted as a function of the coupling as in the empty case, there

are extra effects that are missing in Fig. 2 ($n = 0$): the appearance of an additional pole for $\eta' > 0$. This behaviour is well-reproduced by $D_{MF}(\omega)$, which indicates that the two poles correspond to the exchange of virtual photons with the upper ($n + 1$) and the lower photonic band ($n - 1$), and are not caused by electron-photon correlations (this is also consistent with the fact that for the zeroth photonic band $n = 0$ there is only one pole in the photonic spectral function). Since each band renormalizes differently, the exchange of photons with the upper and lower band are not equivalent processes, and therefore the corresponding poles have their own dependence on ω and η' . For large η' , they both suppress to zero, as for the empty cavity.

There is an additional feature in Fig. 10 that is also missing Fig. 2, and that appears in both the MF and the exact calculation: the presence of abrupt changes in the poles, which are related to the hopping renormalization as a function of η' . This can be easily connected with the dressing of the hopping amplitudes and how they change as a function of η' . The oscillation of the Laguerre polynomials with η' for the non-empty cavity implies that the hopping amplitudes will be effectively suppressed at certain values of the coupling strength, with the subsequent change of sign. While the topology of the chain is determined by the absolute value of the ratio between $t'g'_{nn}$ and tg_{nn} , these changes in the hopping amplitudes are also reflected in the photonic spectral function.

Lastly, panel b) shows additional light-matter resonances that appear in the exact spectral function and that are absent in the MF solution.

* bperez03@ucm.es

† gplatero@icmm.csic.es

‡ a.gomez.leon@csic.es

- [1] M. S. Rudner and N. H. Lindner, *Nature Reviews Physics* **2**, 229 (2020).
- [2] T. Oka and S. Kitamura, *Annual Review of Condensed Matter Physics* **10**, 387 (2019), <https://doi.org/10.1146/annurev-conmatphys-031218-013423>.
- [3] N. H. Lindner, G. Refael, and V. Galitski, *Nature Physics* **7**, 490 (2011), number: 6 Publisher: Nature Publishing Group.
- [4] M. S. Rudner, N. H. Lindner, E. Berg, and M. Levin, *Phys. Rev. X* **3**, 031005 (2013).
- [5] L. D'Alessio and M. Rigol, *Phys. Rev. X* **4**, 041048 (2014).
- [6] M. Bukov, M. Heyl, D. A. Huse, and A. Polkovnikov, *Phys. Rev. B* **93**, 155132 (2016).
- [7] S. A. Weidinger and M. Knap, *Scientific Reports* **7**, 45382 (2017).

- [8] P. Ponte, Z. Papić, F. m. c. Huveneers, and D. A. Abanin, *Phys. Rev. Lett.* **114**, 140401 (2015).
- [9] L. Zhang, V. Khemani, and D. A. Huse, *Phys. Rev. B* **94**, 224202 (2016).
- [10] K. Iwahori and N. Kawakami, *Phys. Rev. A* **95**, 043621 (2017).
- [11] J. W. McIver, B. Schulte, F.-U. Stein, T. Matsuyama, G. Jotzu, G. Meier, and A. Cavalleri, *Nature Physics* **16**, 38 (2020).
- [12] O. Dmytruk and M. Schiro, *Communications Physics* **5**, 271 (2022).
- [13] J. Li, D. Golez, G. Mazza, A. J. Millis, A. Georges, and M. Eckstein, *Phys. Rev. B* **101**, 205140 (2020).
- [14] J. Li, L. Schamrik, and M. Eckstein, *Phys. Rev. B* **105**, 165121 (2022).
- [15] M. A. Sentef, J. Li, F. Künzel, and M. Eckstein, *Phys. Rev. Research* **2**, 033033 (2020).
- [16] M. A. Sentef, J. Li, F. Künzel, and M. Eckstein, *Phys. Rev. Research* **2**, 033033 (2020).
- [17] A. Frisk Kockum, A. Miranowicz, S. De Liberato, S. Savasta, and F. Nori, *Nature Reviews Physics* **1**, 19 (2019), publisher: Springer US.
- [18] T. Niemczyk, F. Deppe, H. Huebl, E. P. Menzel, F. Hocke, M. J. Schwarz, J. J. Garcia-Ripoll, D. Zueco, T. Hümmer, E. Solano, A. Marx, and R. Gross, *Nature Physics* **6**, 772 (2010).
- [19] A. A. Anappara, S. De Liberato, A. Tredicucci, C. Ciuti, G. Biasiol, L. Sorba, and F. Beltram, *Phys. Rev. B* **79**, 201303 (2009).
- [20] D. De Bernardis, P. Pilar, T. Jaako, S. De Liberato, and P. Rabl, *Phys. Rev. A* **98**, 053819 (2018).
- [21] O. Di Stefano, A. Settineri, V. Macrì, L. Garziano, R. Stassi, S. Savasta, and F. Nori, *Nature Physics* **15**, 803 (2019).
- [22] A. Settineri, O. Di Stefano, D. Zueco, S. Hughes, S. Savasta, and F. Nori, *Phys. Rev. Research* **3**, 023079 (2021).
- [23] S. Savasta, O. Di Stefano, A. Settineri, D. Zueco, S. Hughes, and F. Nori, *Phys. Rev. A* **103**, 053703 (2021).
- [24] L. Garziano, A. Settineri, O. Di Stefano, S. Savasta, and F. Nori, *Phys. Rev. A* **102**, 023718 (2020).
- [25] R. P. Feynman, *Phys. Rev.* **84**, 108 (1951).
- [26] W. P. Su, J. R. Schrieffer, and A. J. Heeger, *Phys. Rev. Lett.* **42**, 1698 (1979).
- [27] A. J. Heeger, S. Kivelson, J. R. Schrieffer, and W. P. Su, *Rev. Mod. Phys.* **60**, 781 (1988).
- [28] F. Appugliese, J. Enkner, G. L. Paravicini-Bagliani, M. Beck, C. Reichl, W. Wegscheider, G. Scalari, C. Ciuti, and J. Faist, *Science* **375**, 1030 (2022), <https://www.science.org/doi/pdf/10.1126/science.abl5818>.
- [29] Notice that we have assumed the dipole approximation, where the vector potential does not vary within the scale of the electronic system and its amplitude is independent of the spatial coordinate.
- [30] O. Dmytruk and M. Schiró, *Phys. Rev. B* **103**, 075131 (2021).
- [31] G. D. Mahan, *Many-Particle Physics* (Springer New York, NY, New York, 2000).
- [32] Although the Krummer function is well-defined only for $l \geq s$, a numerical calculation of the exact matrix elements shows that they are symmetric $g_{s,l}^{j,i} = g_{l,s}^{j,i}$.
- [33] A. Gómez-León and G. Platero, *Phys. Rev. Lett.* **110**, 200403 (2013).
- [34] A. Eckardt and E. Anisimovas, *New Journal of Physics* **17**, 093039 (2015).
- [35] J. Li and M. Eckstein, *Phys. Rev. Lett.* **125**, 217402 (2020).
- [36] B. Pérez-González, M. Bello, A. Gómez-León, and G. Platero, *Phys. Rev. B* **99**, 035146 (2019).
- [37] T. Kitagawa, T. Oka, A. Brataas, L. Fu, and E. Demler, *Phys. Rev. B* **84**, 235108 (2011).
- [38] A. Gómez-León, P. Delplace, and G. Platero, *Phys. Rev. B* **89**, 205408 (2014).
- [39] A. Blais, R.-S. Huang, A. Wallraff, S. M. Girvin, and R. J. Schoelkopf, *Phys. Rev. A* **69**, 062320 (2004).
- [40] A. Lupascu, S. Saito, T. Picot, P. C. de Groot, C. J. P. M. Harmans, and J. E. Mooij, *Nature Physics* **3**, 119 (2007).
- [41] T. Nakajima, A. Noiri, J. Yoneda, M. R. Delbecq, P. Stano, T. Otsuka, K. Takeda, S. Amaha, G. Allison, K. Kawasaki, A. Ludwig, A. D. Wieck, D. Loss, and S. Tarucha, *Nature Nanotechnology* **14**, 555 (2019).
- [42] A. Gómez-León, F. Luis, and D. Zueco, *Phys. Rev. Applied* **17**, 064030 (2022).
- [43] B. Pérez-González, I. Gómez-León, and G. Platero, *Phys. Chem. Chem. Phys.* **24**, 15860 (2022).
- [44] M. Leijnse and K. Flensberg, *Phys. Rev. Lett.* **107**, 210502 (2011).
- [45] L. Nicolai and H. P. Büchler, *npj Quantum Information* **3**, 47 (2017).
- [46] M. Bello, C. E. Creffield, and G. Platero, *Scientific Reports* **6**, 22562 (2016).
- [47] M. Bello, C. E. Creffield, and G. Platero, *Phys. Rev. B* **95**, 094303 (2017).
- [48] A. Palacios-Laloy, F. Nguyen, F. Mallet, P. Bertet, D. Vion, and D. Esteve, *Journal of Low Temperature Physics* **151**, 1034 (2008).
- [49] C. Schäfer, M. Ruggenthaler, V. Rokaj, and A. Rubio, *ACS Photonics* **7**, 975 (2020).
- [50] M. Kiffner, J. R. Coulthard, F. Schlawin, A. Ardavan, and D. Jaksch, *Phys. Rev. B* **99**, 085116 (2019).
- [51] G. M. Andolina, F. M. D. Pellegrino, V. Giovannetti, A. H. MacDonald, and M. Polini, *Phys. Rev. B* **100**, 121109 (2019).
- [52] A. Blais, R.-S. Huang, A. Wallraff, S. M. Girvin, and R. J. Schoelkopf, *Phys. Rev. A* **69**, 062320 (2004).
- [53] A. Wallraff, D. I. Schuster, A. Blais, L. Frunzio, J. Majer, M. H. Devoret, S. M. Girvin, and R. J. Schoelkopf, *Phys. Rev. Lett.* **95**, 060501 (2005).
- [54] M. Boissonneault, J. M. Gambetta, and A. Blais, *Phys. Rev. A* **79**, 013819 (2009).
- [55] J. Gambetta, A. Blais, D. I. Schuster, A. Wallraff, L. Frunzio, J. Majer, M. H. Devoret, S. M. Girvin, and R. J. Schoelkopf, *Phys. Rev. A* **74**, 042318 (2006).
- [56] V. Gurarie, *Phys. Rev. B* **83**, 085426 (2011).
- [57] S. R. Manmana, A. M. Essin, R. M. Noack, and V. Gurarie, *Phys. Rev. B* **86**, 205119 (2012).
- [58] A. M. Essin and V. Gurarie, *Phys. Rev. B* **84**, 125132 (2011).
- [59] K. Shiozaki, H. Shapourian, K. Gomi, and S. Ryu, *Phys. Rev. B* **98**, 035151 (2018).
- [60] H. Shapourian, K. Shiozaki, and S. Ryu, *Phys. Rev. Lett.* **118**, 216402 (2017).
- [61] S. Ryu, A. P. Schnyder, A. Furusaki, and A. W. W. Ludwig, *New Journal of Physics* **12**, 065010 (2010).